Rapid synthesis of LiCo$_{1-x}$Fe$_x$PO$_4$/C Cathodes via Microwave Solvothermal Method for Li-ion Batteries

Dongyun Zhang[1,], Jiang Zhou[1], Jie Chen[1], Bingyan Xu[2], Wen Qin[1], Chengkang Chang[1,3,*]*

[1] School of Materials Science and Engineering, Shanghai Institute of Technology, 100 Haiquan Road, Shanghai 201418, China
[2] STATE GRID Shanghai Jinshan Electric Power Supply Company, No.2522, Jinshan Avenue, Shanghai 200540, China
[3] Shanghai Institute of innovative Materials, Shanghai University, 99 Shangda Road, Shanghai 200444, China
[*]E-mail: dyz@sit.edu.cn, ckchang@sit.edu.cn

Olivine-structured LiCo$_{1-x}$Fe$_x$PO$_4$/C (0.2≤x≤0.5) materials were rapidly synthesized via a microwave solvothermal method at 200 °C for 20 min. According to the XRD and SEM mapping results, partial Co sites are successfully substituted with Fe to form a solid solution and expand the Li$^+$ diffusion channel. Both the discharge capacity and cyclic capacity retention as well as the rate capacity of the LiCo$_{1-x}$Fe$_x$PO$_4$/C (0.2≤x≤0.5) samples increase with increasing x. Furthermore, the optimized Fe substitution content should be x=0.4 with respect to the energy density. The LiCo$_{0.5}$Fe$_{0.5}$PO$_4$/C exhibits the highest capacity retention of 87.7% after 50 cycles at 0.5 C, which could result from its high lithium ion diffusion coefficient (D_{Li}) of 1.48×10^{-13} cm^2 s^{-1} and low charge transfer resistance (R$_{ct}$) of 74 Ω based on the EIS results. According to the XPS analysis, Fe^{2+} and a small amount of Fe^{3+} coexist in LiCo$_{0.5}$Fe$_{0.5}$PO$_4$/C. The substitution of Fe^{3+} in the Co^{2+} sites produces Co vacancies accompanied by conduction electrons to maintain the neutrality of the lattice in LiCoPO$_4$, which improves D_{Li} and the bulk electronic conductivity.

1. INTRODUCTION

The excellent performance of LiMPO$_4$ (M=Fe, Mn, Co, Ni) has attracted great attention since discovery by Padhi in 1997 [1]. Olivine-structured LiCoPO$_4$ is often considered one of the most promising cathode materials for LIBs due to its high potential plateau (4.8 V) and high theoretical energy density (802 Wh kg^{-1}) [2]. However, the low initial discharge capacity and poor cycling ability

of LiCoPO$_4$ limit its application [3-8]. Several methods, such as particle downsizing [7, 9-12], carbon coating [6, 13-15] and ions substitution [9, 14, 16] have been employed to solve the above problems. Modification of LiCoPO$_4$ with metal ion substitutions, such as Mn^{2+}, Ca^{2+}, Mg^{2+}, Zn^{2+} and Fe^{2+}, has been proved an effective way [4, 9, 17-19]. Many studies have examined the substituting Fe in the Co site [9, 20-22], which could improve the cycling ability of LiCoPO$_4$ by enlarging its lattice parameters and broadening the lithium ion channel. LiCo$_{1-x}$Fe$_x$PO$_4$ materials have been synthesized by solid phase [23-26], citrate complexation [2, 27], solvothermal [21, 22], sol–gel [20] and template methods [9]. Han [26] synthesized LiCo$_{0.95}$Fe$_{0.05}$PO$_4$ with a discharge capacity of 120 mAh g^{-1} at 0.05 C by ball-milling coupled with microwave heating. Yang [25] obtained Li$_{1.02}$[Co$_{0.9}$Fe$_{0.1}$]$_{0.98}$PO$_4$ with a discharge capacity of 130 mAh g^{-1} at 0.1 C by using a solid-state reaction. Allen [2] prepared Li$_{0.92}$Co$_{0.8}$Fe$_{0.2}$PO$_4$ via a citrate complexation route with microwave drying, which possessed a discharge capacity of 120 mAh g^{-1} at 0.1 C. Li$_{0.973}$(Fe$_{0.1}$Co$_{0.9}$)$_{1.014}$PO$_4$ was prepared at 240 °C over 65 h by a solvothermal method, which had a discharge capacity of 120 mAh g^{-1} at 0.1 C [21]. Singh [20] adopted a microwave-assisted non-aqueous sol–gel method to produce LiCo$_{1-x}$Fe$_x$PO$_4$ cathode materials, which required only 65 min at 270 °C. Recently, Fang [9] reported that LiCo$_{0.8}$Fe$_{0.2}$PO$_4$ nanoplates prepared by a template method showed a discharge capacity of 147 mAh g^{-1} at 0.1 C with a 93.8% capacity retention after 300 cycles. When employed in solid-state method, citrate complexation method or sol–gel method, microwave-assisted heating has proved effective at reducing the synthesis time. The microwave solvothermal method has been used successfully to produce LiCoPO$_4$. Jennifer Ludwig [28] synthesizing LiCoPO$_4$ at 250°C in 30 min by using a microwave solvothermal method. Christoph Neef [29] produced LiCoPO$_4$ via a microwave-assisted hydrothermal method in only 30 s at 220°C. Research has seldom been reported using a microwave solvothermal method to synthesize LiCo$_{1-x}$Fe$_x$PO$_4$.

In this work, we rapidly synthesized LiCo$_{1-x}$Fe$_x$PO$_4$ (0≤x≤0.5) by a microwave solvothermal method within 20 min at 200°C. The effects of Fe substitution on the crystal structure and electrochemical properties of the LiCo$_{1-x}$Fe$_x$PO$_4$ samples were investigated and discussed in detail.

2. EXPERIMENTAL

2.1. Material preparation

The LiCo$_{1-x}$Fe$_x$PO$_4$/C (0≤x≤0.5) samples have been synthesized by microwave solvothermal method following the route presented in reference [30]. However, CoSO$_4$·7H$_2$O (AR,99.5%) was used as a cobalt source, and the reaction temperature was increased to 200 °C from 160°C. The carbon content of the LiCo$_{1-x}$Fe$_x$PO$_4$/C (0≤x≤0.5) materials was kept at 2±0.05%.

2.2. Structural and morphological characterization

The crystalline phase of the obtained powder was identified by XRD (X-ray diffraction experiments, TD3200) using Cu Kα radiation (1.5406 Å) at 40 kV and 30 mA. The XRD data were collected in the range of θ=15–70° with a scanning speed of 0.02°/s. The morphology of the obtained

spherical porous materials was examined using SEM (scanning electron microscope, JEM-6700F). The element distribution was probed by EDS mapping (energy dispersive X-ray spectroscopy, Bruker XFlash 4010). The elemental carbon analysis of the samples was performed by using C-S analysis equipment (HIR-944B).

2.3. Electrochemical tests

The properties of the obtained cathode materials were evaluated with CR2032 coin-type cells using Li metal as the anode. The $LiCo_{1-x}Fe_xPO_4/C$ composite was mixed with super P and polyvinylidene fluoride (PVDF) with a weight ratio of 80:10:10 in N-methyl-2-pyrrolidone (NMP). The cathode slurry was coated on Al foil and dried at 120 °C for 12 h in vacuum. The dried cathode material was pressed and punched into disc with a diameter of 12 mm. The coin-type cells were assembled in a glovebox filled with dry Ar atmosphere. A polypropylene membrane (Celgard 2400) and 1 M $LiPF_6$ (EC:DEC=1:1, vol.%) were used as the separator and electrolyte. The assembled coin-type cells were left for 8 h. Galvanostatic charge/discharge tests were determined under different rates ranging from 0.1C to 10C and cycling performances were carried out in a Land Battery test system (CT2001A, wuhan LAND, China) at a working voltage of 2.5-5.0 V vs. Li^+/Li at room temperature. Electrochemical impedance spectroscopy (EIS) was measured on the electrochemical workstation (Autolab PGSTAT302N) in a frequency range of 500KHz to 0.05 Hz with an amplitude of 5 mV.

3. RESULTS AND DISCUSSION

Fig. 1 shows the XRD patterns of the $LiCo_{1-x}Fe_xPO_4/C$ ($0 \leq x \leq 0.5$) samples prepared by the microwave solvothermal method. According to the patterns of the $LiCoPO_4$ and $LiCo_{0.9}Fe_{0.1}PO_4$ samples, the dominant diffraction peaks could be indexed into the orthorhombic structure of $LiCoPO_4$ with a Pnma space group (PDF#32-0552). In addition, there were some weak impurity peaks, which could be indexed to Li_3PO_4 and $Co_5(PO_4)_2(OH)_4$. When $x \geq 0.2$, the curves of the $LiCo_{1-x}Fe_xPO_4/C$ samples could be indexed into the single $LiCoPO_4$ (PDF#32-0552) phase, and no obvious impurity peak was observed. The diffraction peaks corresponding to crystal plane (311) of the $LiCo_{1-x}Fe_xPO_4/C$ ($0 \leq x \leq 0.5$) samples were amplified in Fig. 1. The diffraction peaks of the (311) crystal plane shifted to left with the Fe content increasing. The specific lattice parameters and unit-cell volumes, determined by the Rietveld refinement method, of all samples are shown in Table 1. It could be found that the crystal lattice parameters and cell volumes mostly decreased with the increasing Fe content from Table.1, which was due to the larger radius of Fe^{2+} (0.78 Å) than Co^{2+} (0.75 Å) [9], indicating that Co^{2+} was successfully substituted by Fe^{2+} to form the solid solutions, resulting in the expansion of the channel for Li^+ migration.
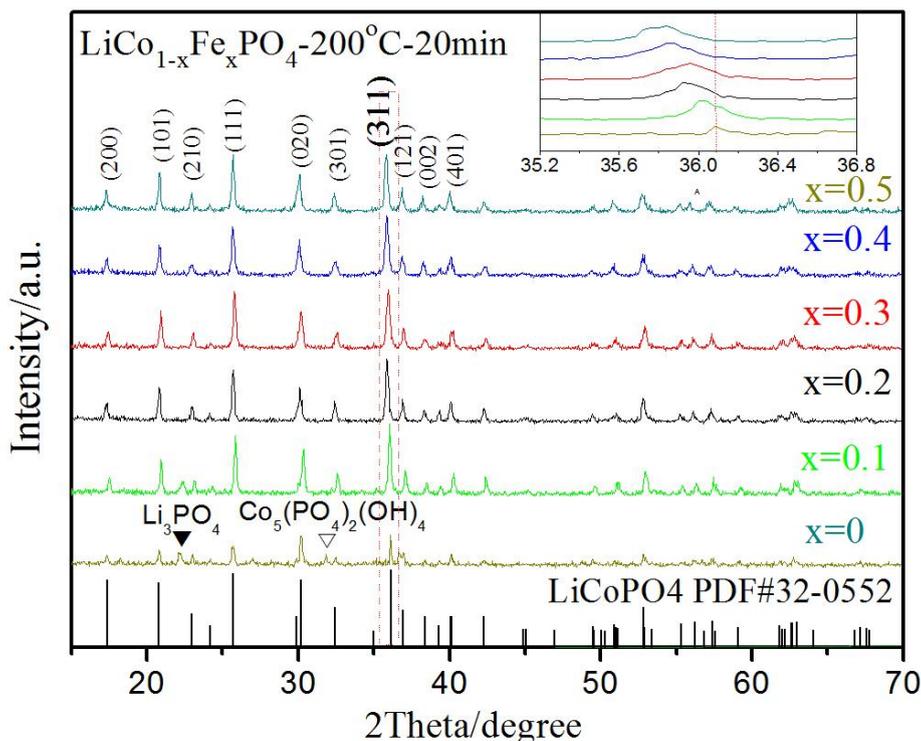
Figure 1. XRD patterns of the $LiCo_{1-x}Fe_xPO_4/C$ ($0 \leq x \leq 0.5$) samples. Inset image: Diffraction peaks of crystal face (311).

Table 1. Lattice parameters of the $LiCo_{1-x}Fe_xPO_4/C$ ($0 \leq x \leq 0.5$) composites obtained from the XRD Rietveld refinement

Samples	Cell parameters(Å)			
	a	b	c	Volume
$LiCoPO_4$	10.2061	5.9223	4.7012	284.1574
$LiCo_{0.9}Fe_{0.1}PO4$	10.2136	5.9290	4.7056	284.9544
$LiCo_{0.8}Fe_{0.2}PO4$	10.2165	5.9365	4.7044	285.3230
$LiCo_{0.7}Fe_{0.3}PO4$	10.2232	5.9469	4.7102	286.3630
$LiCo_{0.6}Fe_{0.4}PO4$	10.2286	5.9483	4.7108	286.6182
$LiCo_{0.5}Fe_{0.5}PO4$	10.2298	5.9523	4.7132	286.9907

A Bruker-AXS 133 eV Xflash 4010 Detector attached to the SEM is used to observe the elemental distribution of the $LiCo_{0.5}Fe_{0.5}PO_4/C$ sample. The monodisperse spherical particles with a size distribution ranging from 1μm to 18μm are observed from Fig. 2 (a). In Fig. 2(b)-(f), the different colors represent different elements. The results illustrate that the elements (Co, Fe, P and O) are uniformly distributed in the $LiCo_{0.5}Fe_{0.5}PO_4/C$ sample. Combined with the XRD results, it can be inferred that Fe enters the crystal lattice of $LiCoPO_4/C$ to form a solid solution.
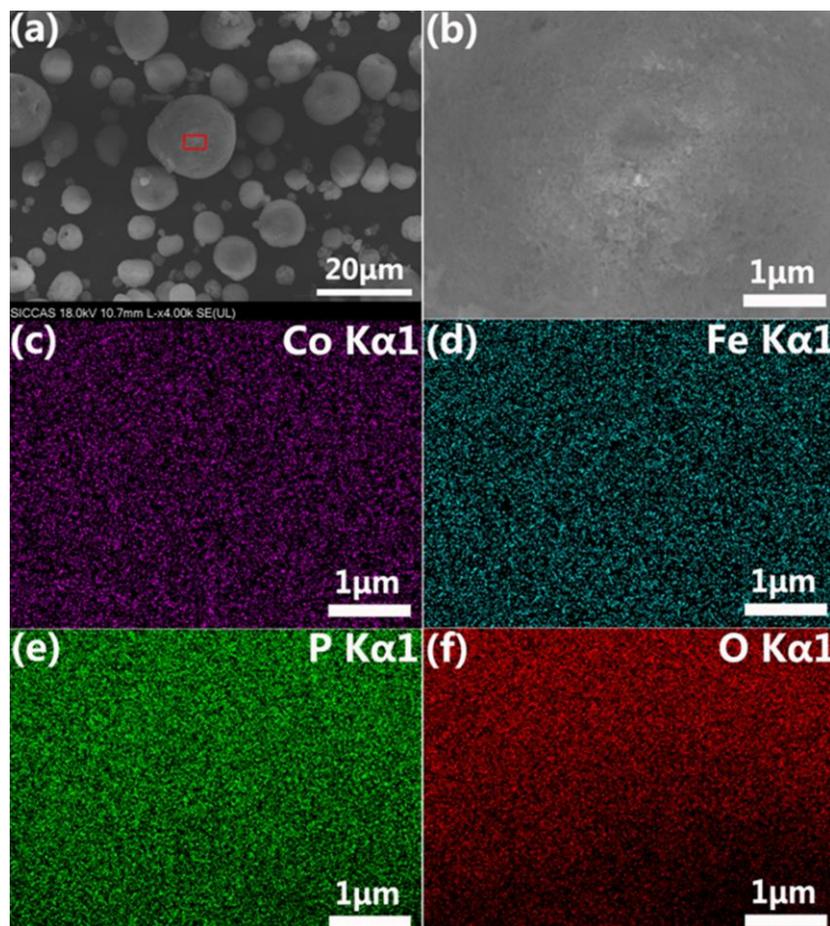
Figure 2. SEM images (a,b) and the elemental mappings of Co (c), Fe (d), P (e) and O (f) for the LiCo$_{0.5}$Fe$_{0.5}$PO$_4$/C sample

The charge/discharge curves of LiCo$_{1-x}$Fe$_x$PO$_4$/C (0.2≤x≤0.5) at 0.1 C are depicted in Fig. 3(a). Obviously, there are two platforms at 3.5 V and 4.7 V emerging from the discharge curves of all the samples, which are ascribed to the Fe^{3+}/Fe^{2+} and Co^{3+}/Co^{2+} redox couples, respectively. The redox couple of Fe^{3+}/Fe^{2+} occurs at a higher potential in LiCo$_{1-x}$Fe$_x$PO$_4$ than in LiFePO$_4$ (3.4 V) [31], and the Co^{3+}/Co^{2+} reduction potential is lower than that in LiCoPO$_4$ (4.8 V) [2]. A similar result was reported by Kosova [24], and it was mentioned that the substitution of the more electropositive Fe^{2+} for Co^{2+} increases the Co-O covalence due to the inductive effect, and thereby raising the Fe^{2+}/Fe^{3+} redox energy and decreasing the voltage of the Co^{2+}/Co^{3+} pair. This phenomenon may give rise to a super exchange interaction between Fe-O-Co ions [32]. Furthermore, the discharge capacity of LiCo$_{1-x}$Fe$_x$PO$_4$/C increases with increasing x. The discharge capacities of the LiCo$_{0.8}$Fe$_{0.2}$PO$_4$/C and LiCo$_{0.7}$Fe$_{0.3}$PO$_4$/C are 69.8 mAh g^{-1} and 75.7 mAh g^{-1}. When x further increases, the discharge capacity of LiCo$_{0.6}$Fe$_{0.4}$PO$_4$/C increases up to 102.1 mAh g^{-1}, which is close to the value of that of the LiCo$_{0.5}$Fe$_{0.5}$PO$_4$/C (102.7 mAh g^{-1}). The discharge capacity increasing with Fe content could result in the enlargement of the 1D Li$^+$ diffusion channels by Fe substitution [24, 25]. This inference is consistent with the XRD results. Fig. 3(b) exhibits the energy density of the LiCo$_{1-x}$Fe$_x$PO$_4$/C (0.2≤x≤0.5) samples. At first, the energy density of the LiCo$_{1-x}$Fe$_x$PO$_4$/C (0.2≤x≤0.4) increases with increasing x. The energy density of LiCo$_{0.8}$Fe$_{0.2}$PO$_4$/C is 306.7 Wh kg^{-1}. When x=0.4, it achieves the

highest value of 422.2 Wh kg^{-1} for the LiCo$_{0.6}$Fe$_{0.4}$PO$_4$/C. Then, for LiCo$_{0.5}$Fe$_{0.5}$PO$_4$/C, it decreases to 405.8 Wh kg^{-1}. Although LiCo$_{0.5}$Fe$_{0.5}$PO$_4$/C exhibits a higher discharge capacity than that of LiCo$_{0.6}$Fe$_{0.4}$PO$_4$/C, it is not enough to compensate for the energy density loss caused by the shortening of the voltage platform at 4.7 V. From the perspective of energy density, no benefit is observed when the amount of Fe substitution is larger than 0.4.
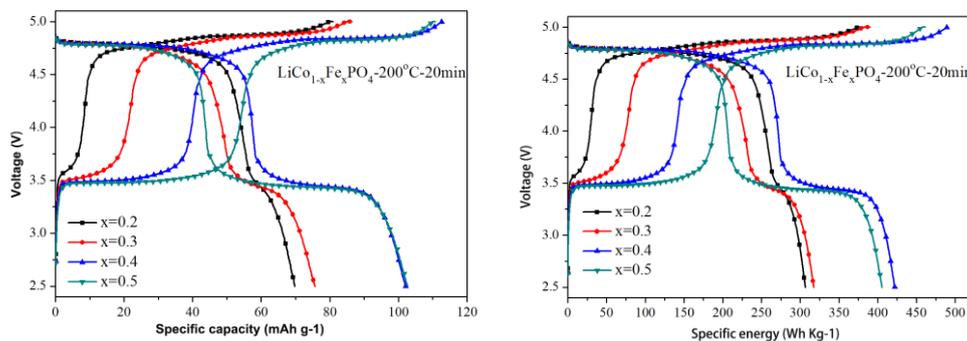
Figure 3. The first charge/discharge profiles of LiCo$_{1-x}$Fe$_x$PO$_4$/C (x≤0.5) at 0.1C (a) capacity-voltage (b) energy-voltage
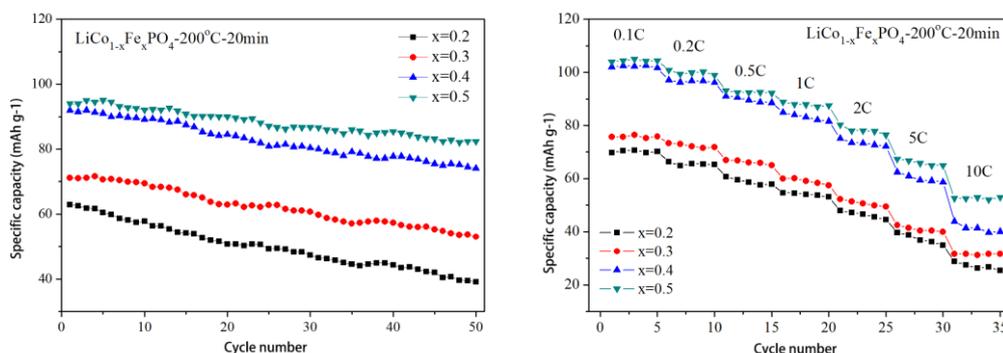
Figure 4. (a) Cycling performance of LiCo$_{1-x}$Fe$_x$PO$_4$/C (0.2≤x≤0.5) at 0.5C, (b) rate performance of LiCo$_{1-x}$Fe$_x$PO$_4$/C (0.2≤x≤0.5) samples at different current densities

The cycling performance of the LiCo$_{1-x}$Fe$_x$PO$_4$/C (0.2≤x≤0.5) samples at 0.5 C is presented in Fig. 4(a). The LiCo$_{0.8}$Fe$_{0.2}$PO$_4$/C sample delivers an initial discharge capacity of 62.9 mAh g^{-1}. With a retention of 62.2% after 50 cycles. As the value of x increases, the discharge capacity and cyclic stability of the LiCo$_{1-x}$Fe$_x$PO$_4$/C (0.2≤x≤0.5) samples increase continually. The discharge capacity of LiCo$_{0.6}$Fe$_{0.4}$PO$_4$/C increases to 92.0 mAh g^{-1} at 0.5 C and remains at 74.1 mAh g^{-1} after 50 cycles. LiCo$_{0.5}$Fe$_{0.5}$PO$_4$/C exhibits an initial discharge capacity of 94.0 mAh g^{-1} at 0.5 C with a retention of 87.7% after 50 cycles, which is superior to the value (78% after 20 cycles at 0.1 C) reported by Lecce [21]. According to Kosova's work [24], the volume changes from 7.0% for LiCoPO$_4$ to 3.7% for LiCo$_{0.5}$Fe$_{0.5}$PO$_4$. The extended cycle life may result from the reduction of the cell volume change and the expansion of the Li$^+$ diffusion channels in LiCo$_{1-x}$Fe$_x$PO$_4$/C during the Li extraction/insertion process, which is caused by the Fe substitution.

Table. 2 Comparison of the electrochemical properties of $LiCoFePO_4/C$ obtained from references [2, 9, 21, 24, 26] and this work

Samples	First discharge / mAh g^{-1}	Capacity retention	Voltage range / V	Reference
$LiCo_{0.5}Fe_{0.5}PO_4$	102.7 (0.1 C)	87.7% after 50 cycles at 0.5 C	2.5-5	this work
Fe doped $LiCoPO_4$ nanoplate	147[*] (0.1 C)	97.9% after 50 cycles at 0.1 C	2.5-4.95	[9]
$LiCo_{0.5}Fe_{0.5}PO_4$	124 (0.1 C)	86.3% after 15 cycles at 0.1 C	3-5	[24]
$Li_{0.973}(Fe_{0.1}Co_{0.9})_{1.014}PO_4$	120 (0.1 C)	78% after 20 cycles at 0.1 C	3.5-5	[21]
$LiCo_{0.95}Fe_{0.05}PO_4$	120[▲] (0.05 C)	—	3.5-5.2	[26]
$LiCo_{0.9}Fe_{0.1}PO_4$	109[▲] (0.05 C)	—	3.5-5.2	[26]
$Li_{0.92}Co_{0.8}Fe_{0.2}PO_4$	120[**] (0.05 C)	<u>80%</u> after 500 cycles at 0.05 C	2.5-5.3	[2]

[*]obtained from the second cycle; [**]obtained from the third cycle; [▲]obtained at 30 ℃

The results in this paper were compared with the results of the references, as shown in Table 2. Recently, Fang [9] reported that Fe-doped $LiCoPO_4$ nanoplates synthesized by a template method exhibited an extremely high capacity of 147 mAhg^{-1} with 97.9% capacity retention after 50 cycles at 0.1 C, and its synthetic process was complicated. $LiCo_{0.5}Fe_{0.5}PO_4$ prepared by Kosova [24] showed an initial discharge capacity of 124 mAhg^{-1} at 0.1 C, which is higher than our result (102.7 mAh g^{-1} at 0.1 C), but it remained at 86.3% of its initial capacity after 15 cycles at 0.1 C. $Li_{0.973}(Fe_{0.1}Co_{0.9})_{1.014}PO_4$ synthesized by Lecce [21] exhibited an initial discharge capacity of 120 mAh g^{-1} with 78% retention after 20 cycles. According to our work, $LiCo_{0.5}Fe_{0.5}PO_4$ displays a capacity retention of 87.7% after 50 cycles at 0.5 C. The $LiCo_{0.95}Fe_{0.05}PO_4$ and $LiCo_{0.9}Fe_{0.1}PO_4$ synthesized by Han [26] displayed discharge capacities of 120 and 109 mAhg^{-1}, respectively, which were tested at 0.05 C and 30 °C. These results were tested at a lower rate and a higher temperature than that of this work. In addition, their capacity retention was not mentioned. Allen [2] reported that $Li_{0.92}Co_{0.8}Fe_{0.2}PO_4$ had a discharge capacity of 120 mAh g^{-1} at the third cycle with a retention of 80% after 500 cycles at 0.05 C. However, they did not exhibit suitable electrochemical properties at a high rate.

To discover the rate capability, different charge/discharge current densities were used for the $LiCo_{1-x}Fe_xPO_4/C$ ($0.2 \leq x \leq 0.5$) samples, and the results are shown in Fig. 4(b). As the Fe content increased, the discharge capacities of the $LiCo_{1-x}Fe_xPO_4/C$ samples increased at all rates ranging from 0.1 C to 10 C. When the x value increased from 0.2 to 0.3, the discharge capacities of the $LiCo_{0.7}Fe_{0.3}PO_4/C$ were slightly higher than that of the $LiCo_{0.8}Fe_{0.2}PO_4/C$. When x=0.4, the discharge

capacity of $LiCo_{0.6}Fe_{0.4}PO_4/C$ at each rate was significantly higher than that of the $LiCo_{0.7}Fe_{0.3}PO_4/C$. The superiority of $LiCo_{0.6}Fe_{0.4}PO_4/C$ held when the rate was no more than 5 C and dropped at 10 C, implying that there might be two different rate-determining factors at low and high rates, respectively, and requiring further study in the following. $LiCo_{0.5}Fe_{0.5}PO_4/C$ exhibited the highest discharge capacity at each rate with a value of 104.0, 100.9, 93.2, 88.9, 80.3, 67.4, and 52.6 mAh g^{-1} corresponding to 0.1 C, 0.2 C, 0.5 C, 1 C, 5 C and 10 C, respectively. Compared to the discharge capacities of $LiCo_{0.6}Fe_{0.4}PO_4/C$, its superiority was slight at low rates and became obvious when the rates increased, implying that partial substitution of Fe for Co may not only result in the expansion of Li^+ path in the $LiCoPO_4$ but also enhance the bulk ionic and electronic conductivity [9, 26, 27].

To get further verify the influence of Fe substitution on the lithium ion diffusion coefficient (D_{Li}), electrochemical impedance spectroscopy (EIS) was performed. The results are given in Fig. 5. Fig. 5(a) shows the Nyquist plots and fitting lines of the $LiCo_{1-x}Fe_xPO_4/C$ ($0.2 \leq x \leq 0.5$) samples after 5 cycles at 0.1 C, and the equivalent circuit is shown in the insert of Fig. 5(a). All the curves are consist of a single semicircle in the high-medium-frequency range and a straight line in the low-frequency range. The intercept of the semicircle on the Z′ axis in high frequency indicates the electrolyte resistance (R_s), the diameter of the semicircle indicates the charge transfer resistance (R_{ct}) on the interface of the electrolyte/electrode, CPE represents the double-layer capacitance and passivation membrane capacitance and Z_w represents the Warburg impedance. As shown in the Table 3, the simulation parameters of the equivalent circuit are obtained by the electrochemical workstation (Autolab PGSTAT302N). R_{ct} is an important kinetics parameter of the electrochemical reaction, which is influenced by the ionic diffusion, the electronic conductivity, the reaction temperature, and so on [33]. The charge transfer resistance (R_{ct}) of the $LiCo_{1-x}Fe_xPO_4/C$ ($0.2 \leq x \leq 0.5$) samples decreased from 121 Ω of the $LiCo_{0.8}Fe_{0.2}PO_4/C$ to 74 Ω of the $LiCo_{0.5}Fe_{0.5}PO_4/C$ as the x value increased, corresponding to the continuously decreasing semicircle diameter. That trend indicates that the Fe substitution could greatly improve the conductivity of $LiCo_{1-x}Fe_xPO_4/C$ and might enhance both the electronic and ionic transport during the lithiation/delithiation reaction. The sloping line at low frequency is associated with the diffusion in the solid phase. The lithium ion diffusion coefficient (D_{Li}) can be calculated according to the following equation [30]:

$$D_{Li} = \frac{R^2 T^2}{2A^2 n^4 F^4 C^2 \sigma^2} \qquad (1)$$

$$Z^{'} = B + \frac{\sigma}{\sqrt{\omega}} \qquad (2)$$

where R represents the gas constant, T is the absolute temperature, A is the electrode area, n represents the number of electrons transferred in the half-reaction for the redox couple, F is the Faraday constant, C is the concentration of lithium ion, B is a constant, ω is the angular frequency, and σ is the Warburg factor, which is related to $Z′$. The linear fitting of $Z′$ vs. $\omega^{-1/2}$ in the low-frequency region from which the slope of σ can be obtained is shown in Fig. 5b. According to Eqs. (1) and (2), the D_{Li} values of the $LiCo_{1-x}Fe_xPO_4/C$ ($0.2 \leq x \leq 0.5$) samples are calculated and listed in Table 3. The D_{Li} of $LiCo_{0.7}Fe_{0.3}PO_4/C$ is 9.02×10^{-14} cm^2 s^{-1}, which is one order of magnitude higher than that of the $LiCo_{0.8}Fe_{0.2}PO_4/C$ (8.13×10^{-15} cm^2 s^{-1}). The R_{ct} of $LiCo_{0.7}Fe_{0.3}PO_4/C$, 102 Ω, is 19 Ω lower than that of $LiCo_{0.8}Fe_{0.2}PO_4/C$, which may be attributed to a significant enhancement of Li^+ diffusion. When x=0.4,

the D_{Li} of the $LiCo_{0.6}Fe_{0.4}PO_4/C$ is 1.43×10^{-13} cm^2 s^{-1}, which is 1.6 times of that of $LiCo_{0.7}Fe_{0.3}PO_4/C$. However, the R_{ct} of the $LiCo_{0.6}Fe_{0.4}PO_4/C$ is 23 Ω lower than $LiCo_{0.7}Fe_{0.3}PO_4/C$, which may be due to the improvement of both the ionic and bulk electronic conductivity by Fe substitution [9, 26, 27]. When the Fe content further increases, the D_{Li} of the $LiCo_{0.5}Fe_{0.5}PO_4/C$ is 1.48×10^{-13} cm^2 s^{-1}, which is 1.03 times of that of the $LiCo_{0.6}Fe_{0.4}PO_4/C$. In addition, the R_{ct} of the $LiCo_{0.5}Fe_{0.5}PO_4/C$ decreases 5 Ω, which may be due to the enhancement of the bulk electronic conductivity. Thus, both the ionic and electronic conductivity could be the dominating factors at low rates (≤5 C). In addition, the electronic conductivity might be the rate-limit factor at 10 C.
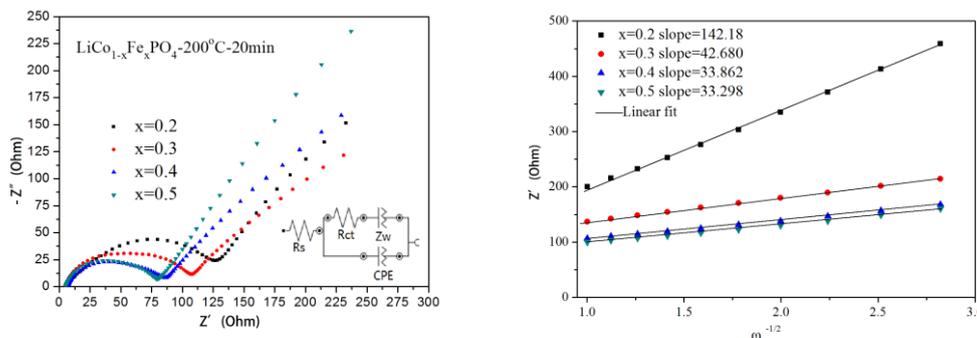
Figure 5. Profiles of electrochemical impedance spectroscopy (EIS). (a) Nyquist curve (b) linear fitting of Z′-ω$^{-1/2}$

Table 3. Resistance of EIS for $LiCo_{1-x}Fe_xPO_4/C$ (0.2≤x≤0.5)

Sample	Rs(Ω)	Rct(Ω)	σ(Ω•s$^{1/2}$)	D_{Li}(cm^2 s^{-1})
$LiCo_{0.8}Fe_{0.2}PO_4/C$	5.19	121	142.18	8.13×10^{-15}
$LiCo_{0.7}Fe_{0.3}PO_4/C$	4.83	102	42.680	9.02×10^{-14}
$LiCo_{0.6}Fe_{0.4}PO_4/C$	5.95	79	33.862	1.43×10^{-13}
$LiCo_{0.5}Fe_{0.5}PO_4/C$	5.62	74	33.298	1.48×10^{-13}
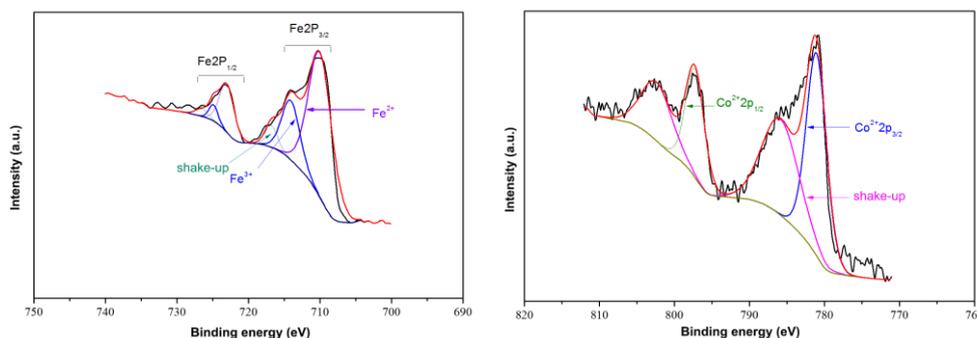
Figure 6. (a) Fe2p and (b) Co 2p XPS spectra of the $LiCo_{0.5}Fe_{0.5}PO_4/C$

The chemical states of Fe and Co in $LiCo_{0.5}Fe_{0.5}PO_4/C$ are performed in the Fig. 6(a).and Fig. 6(b) respectively. The Fe 2p is obviously resolved into Fe (2p$_{3/2}$) and Fe (2p$_{1/2}$) contributions, focused on 709.9, 714.6, 723.8 and 724.9eV. The binding energies 709.9eV and 723.8eV belong to the

characteristic peak of Fe^{2+}, and the others correspond to Fe^{3+}. The clear weak peaks of the shake-up feature in the high-resolution spectrum for Fe, as shown in Fig. 6(a), suggests that all Fe atoms are in the structure of $LiCoPO_4$ [34]. The content of Fe^{3+} is approximately 15%, which may contribute to the synthesis process. The Co 2p is obviously resolved into Co ($2p_{3/2}$) and Co ($2p_{1/2}$) contributions, centered at 781.8 and 798.1eV, respectively. These peaks belong to Co^{2+}. When Co^{2+} is substituted by Fe^{3+}, Co vacancies would be made to balance the valence. The valence balance model is described as Eq. (3):

$$Fe_2O_3 \xrightarrow{CoO} 2Fe_{Co}^{\cdot} + V_{Co}^{''} + 3O_o \qquad (3)$$
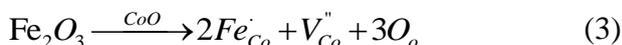
Fe^{3+} substitution at Co^{2+} sites increases the concentration of ionic vacancies according to Eq. (3). To keep neutrality of the lattice in $LiCoPO_4$, conduction electrons are produced to balance the Fe^{3+}, facilitating Li-ion diffusivity and electron conduction during the charge/discharge process [9, 20, 34, 35].

4. CONCLUSIONS

In summary, $LiCo_{1-x}Fe_xPO_4/C$ ($0 \leq x \leq 0.5$) samples were rapidly synthesized by a microwave solvothermal method at 200 °C for 20 min. According to the XRD and SEM mapping results, Co were partially substituted by Fe to form the solid solutions. Based on the Rietveld refinement results, the crystal lattice parameters and cell volumes mostly decreased with the increase in Fe content, which is contributed to the larger radius of Fe^{2+} (0.78 Å) than Co^{2+} (0.75 Å) and results in the expansion of the channel for Li^+ migration. The discharge capacities of the $LiCo_{1-x}Fe_xPO_4/C$ ($0.2 \leq x \leq 0.5$) samples increase with increasing Fe content. However, the optimized Fe substitution content should be x=0.4 in the perspective of energy density. $LiCo_{0.5}Fe_{0.5}PO_4/C$ exhibited outstanding cycle stability with a capacity retention of 87.7% after 50 cycles at 0.5 C, as well as the highest rate capacity. According to the EIS results, the D_{Li} of the $LiCo_{1-x}Fe_xPO_4/C$ samples increased, and the R_{ct} decreased with increasing Fe content. $LiCo_{0.5}Fe_{0.5}PO_4/C$ shows the highest D_{Li} (1.48×10^{-13} cm^2 s^{-1}) and the lowest R_{ct} (74 Ω). Based on the XPS results, Fe^{2+} and a small amount Fe^{3+} coexist in $LiCo_{0.5}Fe_{0.5}PO_4/C$. Fe^{3+} substitution at the Co^{2+} sites lead to the production of Co vacancies with accompanying conduction electrons to maintain neutrality of the lattice in $LiCoPO_4$, which is beneficial for the improvement of D_{Li} and the bulk electronic conductivity.

References

1. A.K. Padhi, K.S. Nanjundaswamy, J.B. Goodenough, *J. Electrochem. Soc*, 144 (1997) 1188-1194.
2. J.L. Allen, T.R. Jow, J. Wolfenstine, *Journal of Power Sources*, 196 (2011) 8656-8661.

3. X. Lin, Y. Ma, J. Wan, Y. Wang, *Chemical Engineering Journal*, 315 (2017) 304-314.
4. N.V. Kosova, O.A. Podgornova, I.A. Bobrikov, V.V. Kaichev, A.V. Bukhtiyarov, *Materials Science and Engineering:* B, 213 (2016) 105-113.
5. T. Fukutsuka, T. Nakagawa, K. Miyazaki, T. Abe, *Journal of Power Sources*, 306 (2016) 753-757.
6. Y. Maeyoshi, S. Miyamoto, H. Munakata, K. Kanamura, *Journal of Power Sources*, 350 (2017) 103-108.
7. B. Wu, H. Xu, D. Mu, L. Shi, B. Jiang, L. Gai, L. Wang, Q. Liu, L. Ben, F. Wu, *Journal of Power Sources*, 304 (2016) 181-188.
8. F. Wang, J. Yang, Y. NuLi, J. Wang, *Journal of Power Sources*, 196 (2011) 4806-4810.
9. L. Fang, H. Zhang, Y. Zhang, L. Liu, Y. Wang, *Journal of Power Sources*, 312 (2016) 101-108.
10. H. Chen, M. Chen, C. Du, Y. Cui, P. Zuo, X. Cheng, G. Yin, *Materials Chemistry and Physics*, 171 (2016) 6-10.
11. J. Wolfenstine, J.L. Allen, T.R. Jow, T. Thompson, J. Sakamoto, H. Jo, H. Choe, *Ceramics International,* 40 (2014) 13673-13677.
12. J. Ludwig, D. Nordlund, M.M. Doeff, T. Nilges, *Journal of Solid State Chemistry*, 248 (2017) 9-17.
13. E. Nanini-Maury, J. Światowska, A. Chagnes, S. Zanna, P. Tran-Van, P. Marcus, M. Cassir, *Electrochimica Acta*, 115 (2014) 223-233.
14. H. Li, Y. Wang, X. Yang, L. Liu, L. Chen, J. Wei, *Solid State Ionics*, 255 (2014) 84-88.
15. R. Sharabi, E. Markevich, V. Borgel, G. Salitra, D. Aurbach, G. Semrau, M.A. Schmidt, N. Schall, C. Stinner, *Electrochemistry Communications*, 13 (2011) 800-802.
16. L. Gao, Z. Xu, S. Zhang, J. Xu, K. Tang, *Solid State Ionics*, 305 (2017) 52-56.
17. A. Örnek, M. Can, A. Yeşildağ, *Materials Characterization*, 116 (2016) 76-83.
18. S. Karthickprabhu, G. Hirankumar, A. Maheswaran, R.S. Daries Bella, C. Sanjeeviraja, *Journal of Electrostatics,* 72 (2014) 181-186.
19. L. Dimesso, D. Becker, C. Spanheimer, W. Jaegermann, *Progress in Solid State Chemistry*, 42 (2014) 184-190.
20. V. Singh, Y. Gershinsky, M. Kosa, M. Dixit, D. Zitoun, D.T. Major, *Physical chemistry chemical physics* : PCCP, 17 (2015) 31202-31215.
21. D. Di Lecce, J. Manzi, F.M. Vitucci, A. De Bonis, S. Panero, S. Brutti, *Electrochimica Acta*, 185 (2015) 17-27.
22. D. Di Lecce, S. Brutti, S. Panero, J. Hassoun, *Materials Letters,* 139 (2015) 329-332.
23. J.L. Allen, J.L. Allen, T. Thompson, S.A. Delp, J. Wolfenstine, T.R. Jow, *Journal of Power Sources*, 327 (2016) 229-234.
24. N.V. Kosova, O.A. Podgornova, E.T. Devyatkina, V.R. Podugolnikov, S.A. Petrov, *J. Mater. Chem. A*, 2 (2014) 20697-20705.
25. S.M.G. Yang, V. Aravindan, W.I. Cho, D.R. Chang, H.S. Kim, Y.S. Lee, *Journal of the Electrochemical Society*, 159 (2012) A1013-A1018.
26. D.-W. Han, Y.-M. Kang, R.-Z. Yin, M.-S. Song, H.-S. Kwon, *Electrochemistry Communications*, 11 (2009) 137-140.
27. J.L. Allen, T. Thompson, J. Sakamoto, C.R. Becker, T.R. Jow, J. Wolfenstine, *Journal of Power Sources,* 254 (2014) 204-208.
28. J. Ludwig, D. Haering, M.M. Doeff, T. Nilges, *Solid State Sciences*, 65 (2017) 100-109.
29. C. Neef, H.-P. Meyer, R. Klingeler, *Solid State Sciences*, 48 (2015) 270-277.
30. J. Chen, D. Zhang, J. Qiao, C. Chang, *Ionics,* (2017).
31. M. Singh, B. Singh, M. Willert-Porada, *Journal of Electroanalytical Chemistry*, 790 (2017) 11-19.
32. H. Li, Y. Li, L. Chen, H. Jiang, J. Wei, H. Wang, Y. Wang, *Journal of Alloys and Compounds*, 617 (2014) 154-159.
33. L. Liao, P. Zuo, Y. Ma, X. Chen, Y. An, Y. Gao, G. Yin, *Electrochimica Acta*, 60 (2012) 269-273.
34. X. Dong, C. Huang, Q. Jin, J. Zhou, P. Feng , F. Shi and D. Zhang, *RSC Adv*, 7 (2017) 33745-33750.

35. H.C. Shin, S.B. Park, H. Jang, K.Y. Chung, W.I. Cho, C.S. Kim, B.W. Cho, *Electrochimica Acta*, 53 (2008) 7946-7951.